Supporting Information

High Q-Factor Plasmonic Surface Lattice Resonances in Colloidal Nanoparticle Arrays

Xiaoyu Qi†, Luis Alberto Pérez†*, Maria Isabel Alonso and Agustín Mihi*

1: Institute of Materials Science of Barcelona, ICMAB-CSIC, Campus de la UAB, 08193 Bellaterra, Catalonia, Spain

†These authors contributed equally to this work.

Corresponding authors: lperez@icmab.es, amihi@icmab.es

Index

1. Materials

Hydrogen tetrachloroaurate trihydrate ($HAuCl_4 \cdot 3H_2O$, ≥ 99.9%, CAS: 16961-25-4, Lot #MKCP1782), hexadecyltrimethylammonium chloride (CTAC, 25 wt% in water, CAS: 112-02-7, Lot #STBJ9502), ethylene glycol (CAS: 107-21-1, Lot #STBK1878), poly ethylene glycol methyl ether thiol (PEG-SH, MW 6000 g/mol, MW 2000 g/mol, Lot #MKCK7227) and trichloro (1H,1H,2H,2H-perfluorooctyl) silane (97%, Lot 0000188010) were purchased from Sigma-Aldrich. L-ascorbic acid (AA, ≥ 99%, CAS: 50-81-7, Lot #Y01E050) was purchased from Alfa Aesar. Sodium borohydride ($NaBH_4$, 99%, CAS: 16940-56-2, Lot A0385677) and sodium hypochlorite (HCLO, 10-15% active chlorine, CAS: 7681-52-0, Lot A0408704) were purchased from Acros Organics. OrmoStamp (Lot 37416) was purchased from Micro Resist Technology. Acetone (≥ 99.6%, CAS: 67-64-1), 2-propanol (≥ 99.9%, CAS: 67-63-0) and ethanol (≥ 96%, CAS: 64-17-5) were purchased from Labbox. Polydimethylsiloxane (PDMS, Sylgard 184) was purchased from Dow Corning (Michigan, USA). Immersion oil IMMOIL-F30CC was purchased from Olympus. SU8-50 was purchased from Kayaku advanced materials. All chemicals were used as received. Milli-Q water (resistivity 18.2 MΩ·cm at 25 ºC) was used in all experiments. Glass substrates (Labbox Spain, 20×20/24×24 mm^2) for assembly were sonicated with acetone and isopropanol for 10 min each, and irradiated by UV-ozone for 10 min. The other glassware was washed with aqua regia (3:1 $HCl:HNO_3$) and Milli-Q water, and dried before use.

2. Synthesis of gold nanoparticles

The synthesis method of gold nanoparticles (NPs) is similar to the early work by Hanske,[1] which is mainly divided into four parts.

2.1 Gold seeds

$NaBH_4$ was used as reductant. Firstly, 50 μL of 50 mM $HAuCl_4$ solution was added to 5 mL of 0.1 M CTAC solution. Then, under vigorous stirring, 200 μL of 20 mM freshly prepared $NaBH_4$ solution was injected. After 3 min, the mixture was diluted 10 times with 100 mM CTAC solution.

2.2 10 nm gold spheres

AA was used as reductant, 900 μL of the previous seeds solution was added to 10 mL of 25 mM CTAC solution, followed by 40 μL of 100 mM AA solution. Under vigorous stirring, 50 μL of 50 mM $HAuCl_4$ solution was added to initiate the growth. The mixture was left undisturbed at room temperature for at least 10 min.

2.3 Seeds growth

In this step, two different sizes of gold NPs were produced. An aliquot of 10 nm gold spheres solution (the volume depends on the desired NPs size) was added to 100 mL of 25 mM CTAC solution (Table S1). Under vigorous stirring, both 250 μL of 100 mM AA and 250 μL of 50 mM $HAuCl_4$ were added, and kept 5 min. Then, the mixture was left undisturbed at room temperature at least 1 h.

2.4 Oxidative etching

The growth solution was heated to 30-35 ºC, and HClO (1-1.5 wt%) was added according to Table S1. 5 min later, different volumes of 50 mM $HAuCl_4$ solution were added (Table S1). The product was monitored every 10 min by UV visible spectroscopy (extinction at 400 nm), until the extinction no longer changed, then the etching process was terminated.

Finally, synthetized gold NPs solution was centrifuged to eliminate unreacted reagents, the surfactant concentration is set to 1 mM CTAC. The resulting colloids can be stored for long periods without visible modifications.

Table S1: Reagents volume, etching and centrifugation parameters of gold nanoparticles synthesis.

Diameter (nm)	Volume of 10 nm gold spheres (μL)	Oxidative etching	Time of etching (min)	Centrifuge velocity (rpm)
30	3500	50 μL HCLO	20	12000
115	70	50 μL HCLO and 37.5 μL $HAuCl_4$	150	3500

3. Nanoparticles surface functionalization

For ligand exchange, 100 μL of 50 mg/mL PEG-SH aqueous solution was reacted with above gold NPs solution. 300 μM CTAC was used as supplementary solution to make the whole volume to 5 mL, and the mixture was left overnight. The next day, the solution was centrifuged 3 times to clean the leftover PEG-SH, and dissolved in 300 μM CTAC solution to calculated concentration of Au^0.[2]

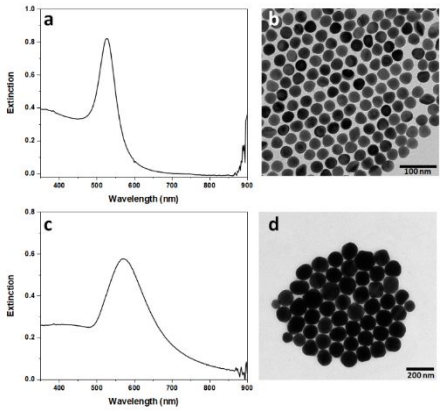

Figure S1 *Extinction spectra and TEM images of the PEG bond - Au NPs dispersion. Size: a, b) (30 ± 2) nm, c, d) (115 ± 20) nm.*

4. Fabrication of PDMS stamps

4.1. Preparation of original master

Silicon substrates patterned with hole arrays (masters) were used as purchased from Eulitha AG (Switzerland), CEMITEC (Spain), and Thunder NIL S.r.l. (Italy), see Table S2 for details. The masters were silanized with an anti-sticking layer by trichloro (1H,1H,2H,2H-perfluorooctyl) silane to prevent the adhesion of silicones and photoresists during replication. In short, the masters were kept under vacuum with 2 µL trichloro (1H,1H,2H,2H-perfluorooctyl) silane in the desiccator for 20 min.

Table S2: Master list

Lattice	Height (nm)	Lattice Parameter (LP) (nm)	Hole Diameter (nm)
square	150	520/560/580/740/780/ 1000/1060/1100/1140/1600/ 1660/1700	260/280/300/440/480/ 600/640/660/700/960/ 1000/1020
square	390	400	150/230
square	390	500	170/277/298
square	390	600	250/338
hexagonal	390	600/700/800	295/335/367

4.2. Preparation of working master

The intermediate master is a negative replica of the original master, and it is used to obtain a stamp made in PDMS. The replica masters were prepared by nanoimprinting technique. Specifically, the OrmoStamp (a photosensitive resist) was dropcasted directly on the silicon master wafer (heated at 60 °C). Then, a clean glass slide was placed on top of this silicon master and gently pressed to make sure no bubbles remain between the glass and OrmoStamp. The photoresist was then cross-linked and hardened under ultraviolet lamp for 10 min. To release the OrmoStamp working master, the glass-silicon master structure was put onto a hot plate where temperature ramps between 110 °C to 180 °C were performed. The thermal expansion difference between the photoresist and the silicon caused the OrmoStamp mold to detach. Finally, the working master was silanized, as previously explained for the original master.[3]

4.3. Fabrication of PDMS molds

Soft PDMS molds were used for all patterns. In short, a 9:1 mixture of the monomer and curing agent were mixed vigorously and degassed under vacuum for 30 min to eliminate bubbles. Then, the mixture was gently poured onto the above working master and left degassing for 30 min. Next, the polymer was cured at 110 °C for 2 h.

5. Fabrication of plasmonic arrays

5.1. Preparation of the assembly

Before assembly, all glass substrates were cleaned by sonication in acetone and isopropanol for 10 min each, and irradiated by UV-ozone for 10 min.

The above gold colloids solution was configured with the same concentration (depending on the desired assembly, the concentration of Au^0 was set to 10-50 mM) by mixture (H_2O 60%, ethanol 40% and final concentration of CTAC was (50-150) μM).

5.2. Template-assisted assembly

1 μL drop of the gold NPs solution was deposited on top of the cleaned glass. Immediately, the drop was covered with the PDMS mold, and the solvent left to evaporate overnight. Next day, PDMS was removed, leaving the gold nanocrystals assembly on the glass. Normally, the PDMS mold could be reused after cleaning with adhesive tape, ethanol and water.

6. Index matching

Immersion Oil Type –F (Olympus) was used as index match medium, when glass substrates were used. 5 μL oil was dropped on top of the plasmonic array. Immediately, a clean glass coverslip was gently placed on top of the oil, evenly spreading all the oil over the entire surface. When PDMS or SU8-50 were used, the index match was done using the same substrate material.

7. Morphological characterization – TEM, SEM

Transmission electron microscopy (TEM) images were collected by JEOL 1210 TEM instrument (Tokyo, Japan) operating at 120 kV. 200 mesh carbon film Cu grids were purchased from Electron Microscopy Science. Scanning electron microscopy (SEM) images were collected by FEI QUANTA 200 Field Emission Gun, operating at 15 kV. As the samples are non-conductive, low vacuum (60 Pa) was used in a water vapor atmosphere. Working distance was (8 - 10) mm.

8. Optical properties measurements

Optical Characterization – UV-visible

NPs dispersion extinction spectra were recorded by Hitachi U-3000 spectrophotometer. Wavelength range: (350 - 900) nm. Polystyrene cuvettes with 1 cm path length were used.

Optical Characterization – Visible/NIR

A Fourier-transform infrared (FTIR) spectrometer Vertex 70 Bruker Hyperion FTIR spectrometer (Bruker, USA), was used for optical transmittance measurements. The resolution and spectral averaging were (8 - 32) cm^{-1}, and (200 - 500) scans, respectively. For the characterization of the NA influence on the optical transmittance 10x NA: 0.25, 4x NA: 0.10, 2x NA: 0.05 objectives were used to focalize light on the sample, and 4x NA: 0.1 in the collection. No objectives were used in the remaining experiments.

Optical Characterization—Coherent Source

A supercontinuum laser source (Fianium SC400) was used for coherent transmittance measurements. The supercontinuum laser is coupled to a monocromator (Fianium LLTFCONTRAST™) (400 - 1000 nm), spectral bandwidth 2.5 nm. The transmitted light was measured as the ratio of the photocurrent intensity (ThorLabs 50 mW, 200 - 1100 nm) obtained with the sample normalized to that of clean glass, acting as a reference.

Angular Resolved Transmittance Characterization —Optical Bench

Transmittance measurements were collected with a custom-built setup on an optical bench consisting of a light source, optical components for alignment, and signal collection and measurement. Briefly, a Tungsten Halogen Lamp (Ocean Optics, HL-2000-HP, Florida, USA) was used as light source; before the sample, the beam passes through an iris with ≈ 1.5 mm aperture, determining the spot size of the excitation light; samples were placed on a rotational stage (Thorlabs, RP03/M, New Jersey, USA) to vary the illumination angle of incidence (AOI). Transmitted light was then collected by a fiber coupled spectrophotometer (Ocean Insight, QEPro-FL or NIR-Quest, depending on the spectral range). Air was used as reference. In order to obtain angle-resolved transmittance maps, transmittance spectra were taken varying the angle of incidence from -45º to +45º with 1º step. The collected data was processed to create a visual representation of transmittance as a function of both wavelength and angle.

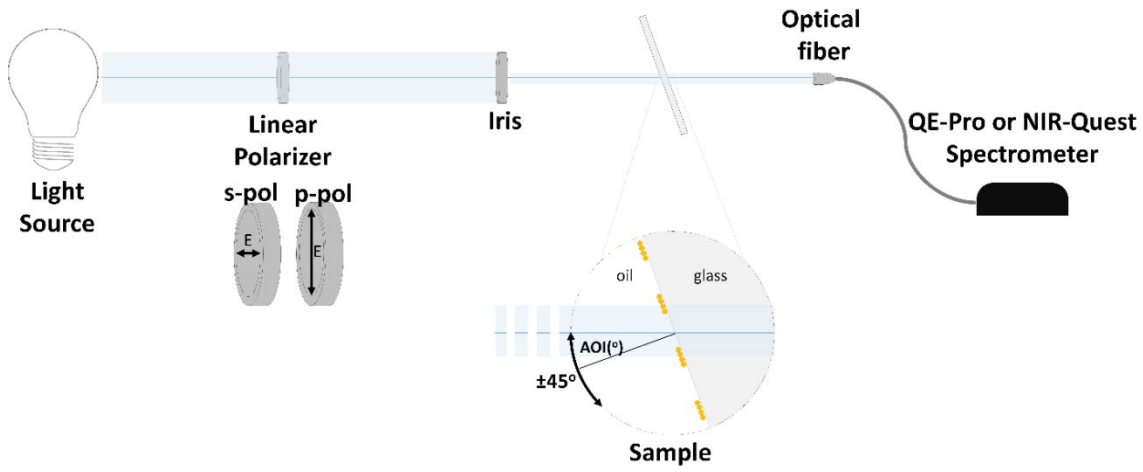

Figure S2 *Schematic representation of the setup used for the angle resolved optical characterization. A tungsten halogen lamp (Ocean Insight, HL-2000-HP) was used as light source. A linear polarizer allowed to choose s or p polarization from the unpolarized light emitted by the lamp. Experiments were conducted with light polarized parallel to the rotation axis (s-polarized) and perpendicular to it (p-polarized). In the first-order diffraction, this allows distinguishing between the states (±1, 0) and (0, ±1). Subsequently, the beam passes through an iris with ≈ 1.5 mm aperture. The sample is mounted on a rotator, and the experiments were performed up to a maximum angle of incidence (AOI) of ± 45°. Finally, the light is collected by an optical fiber and directed to a spectrophotometer. Depending on the spectral region, a QE-Pro or NIR-Quest, both from Ocean Insight, were used.*

9. Numerical Simulations - FDTD

All simulations were performed with the Finite Difference Time Domain (FDTD) commercial software (Ansys FDTD-Solutions, Lumerical). Periodic boundary conditions were imposed at the grating plane and perfect-matched layer in the normal axis. A single sphere of 115 nm and sphere dimers and trimers (2 nm gap) were considered to model single nanoparticle experiments. For 28 nm diameter NPs, 19 and 37 close packed NPs clusters (2 nm gap) were considered placed at the interface between two media (substrate and superstrate).

10. Adaptability of template assisted self-assembly on various substrates

Template assisted self-assembly shows an excellent adaptability to different substrates including stretchable and flexible substrates. In figure S3 the transmittance spectra of meta-molecule arrays (NPs 30 nm) are shown for PDMS, glass and SU8-50 substrates (the thickness of each substrate is (0.2 - 1) mm. The arrays are then index matched using the same materials of the substrate, except

in the glass where oil is used as index match medium. Well resolved Surface Lattice Resonances (SLRs) are observed in all samples. The SLR spectral position shifts according to the substrate refractive index. λ_R = 695 nm for PDMS (n = 1.411 at λ_R), λ_R = 743 nm for glass (n = 1.48 at λ_R) and λ_R = 775 nm for SU8-50 (n = 1.56 at λ_R). The Q-factor for glass and SU8-50, are 102 and 80 respectively, whereas in PDMS the SLR is closer to the Localized Surface Plasmon Resonance (LSPR) leading to a bigger FWHM, hence lower Q-factor (Q = 44).

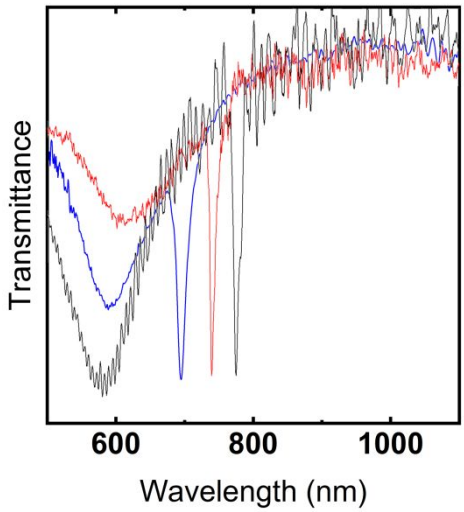

Figure S3 *Experimental transmittance spectra at normal incidence of plasmonic meta-molecule arrays: 30 nm nanoparticle clusters. The lattice parameter is 500 nm. The substrate/superstrate is PDMS/PDMS (blue line), Glass/oil (red line) and SU8-50/SU8-50 (black line).*

11. Impact of numerical aperture on spectral profiles in meta-molecule arrays

The spectral profile, when measuring the optical properties of meta-molecule arrays, and lattices in general, are highly dependent on the instrumental parameters used during the measurement, as an example, the transmittance spectra for a lattice parameter (LP) = 500 nm, 30 nm NP clusters arrays, are shown in Figure S4a, the measurement was done in the same sample region, with the same collection optics, the difference between the spectra is the numerical aperture (NA) of the incidence optics. Whereas the black curve exhibits a narrow and resolved SLR, the blue curve shows a much wider and lower amplitude SLR. As shown in Figure S4b, the Q-factor values decrease as the incidence NA increases. This is because, with an increase in the angle of the incident light cone, the spectral position of the SLR becomes broad. Additionally, it can be observed that the first-order Rayleigh Anomaly (RA) is prominent in all four curves near 740 nm, whereas the weak second-order RA (520 nm) loses intensity and becomes imperceptible.

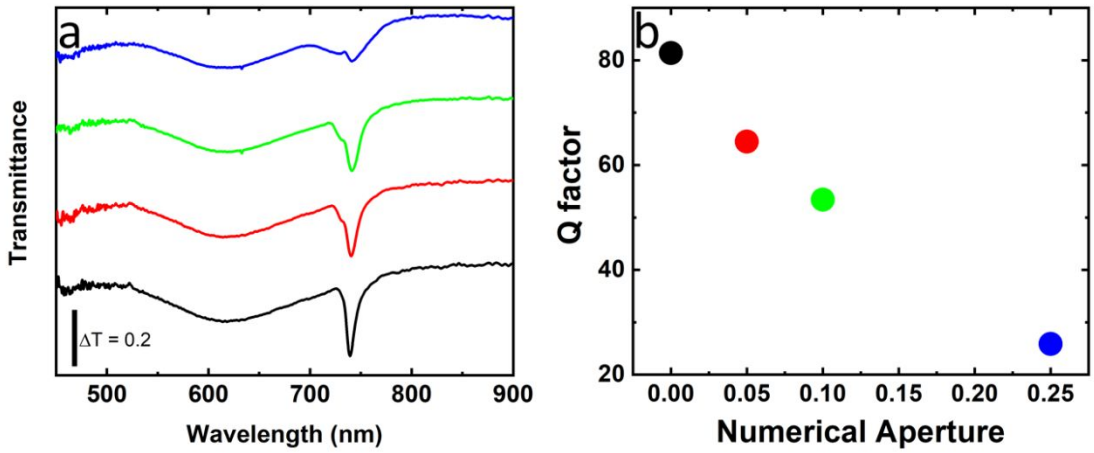

Figure S4. *a) Experimental transmittance spectra at normal incidence of plasmonic meta-molecule arrays: 30 nm nanoparticle clusters. The lattice parameter is 500 nm. The incidence optics NA is: ≈ 0 (no optics) (black line), 0.05 (red line), 0.1 (green line) and 0.25 (blue line). b) Q factor values for each spectrum, the dot color corresponds to the line color.*

12. Challenges and factors affecting the quality factor in single nanoparticle arrays: insights into fabrication.

Achieving a good quality single nanoparticle array is quite challenging, there are several aspects that lead to a significant decrease in the expected Q-factor:

1) ***Finite areas***: depending on the fabrication methodology, sample areas range from a few square micrometers to square centimeters, with the latter considered in most cases as quasi-infinite.[4-6]

2) ***Size and shape dispersion of colloidal particles***: since the LSPR of each particle depends on its morphology, dispersion in size and shape, directly affects the quality of the SLR.[7] Nevertheless, the development of specialized synthesis methods has significantly improved the level of monodispersity in colloids, making it highly acceptable.[1]

3) ***Heterogeneous dielectric environment***: as is described below (Figure 5) the index matching between the substrate and the superstrate in the array can strongly affect the resulting optical properties.[8]

4) ***Defects and disorder***: vacancies in the array and the loss of long-range order are common causes of decreased quality factor in bottom up methods.[9]

5***) Multiplicity of particles per unit cell***: near-field coupling between NPs strongly affects their LSPR, thereby influencing the properties of the SLR, particularly for medium to large-sized particles in small LPs (Figure 2, and S5).

When molds with holes much larger than the colloids are utilized, it is highly probable to obtain multiple NPs in each hole, forming clusters. As shown in Figure S5a, these clusters predominantly

consist of dimers, trimers, tetramers, and larger clusters within each unit cell. The strong near-field coupling between the larger NPs leads to a significant red shift of the cluster's LSPR in the range of 800 - 900 nm (Figure S5c). Additionally, after index matching, a slight increase in transmittance at the Rayleigh anomaly (λ_{RA}) and a shoulder at the surface lattice resonance (λ_{SLR}) can be observed. To reduce the density of clusters, a lower concentration colloidal solution was used, as shown in Figure S5b mainly dimers, trimers, and a few tetramers, along with a significant number of single NPs. However, as a drawback, a considerable number of vacancies (approximately 35%) are observed. The optical properties of these structures, after index matching, exhibit a faint yet resolved SLR and a distinct RA. Furthermore, a LSPR band located at 900 nm is observed due to the presence of aggregates. This observation is in agreement with electrodynamic modeling of dimeric and trimeric structures (Figure S5e), where both features are present: a faint SLR and at longer wavelengths, an intense aggregate band.

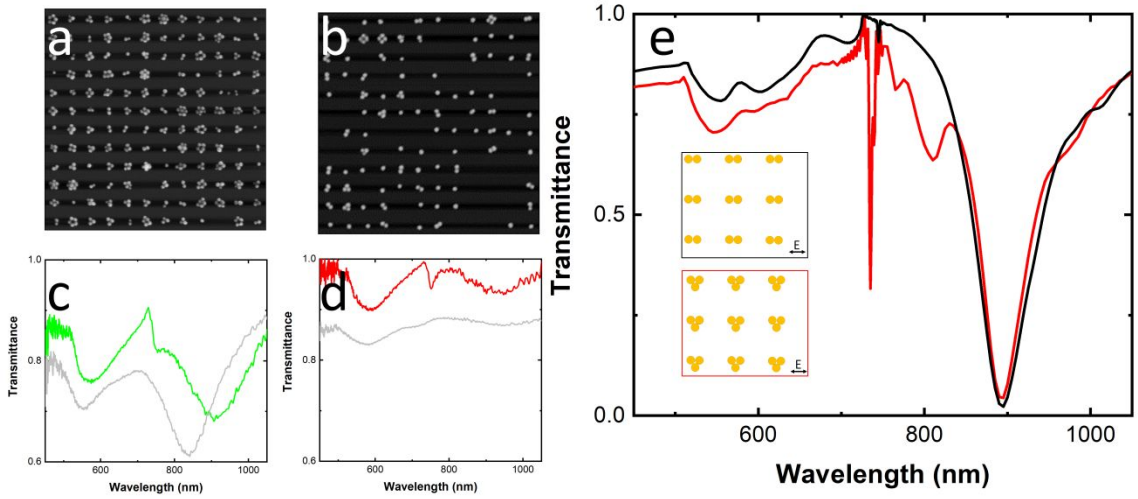

Figure S5 *a, b) SEM images and c, d) Experimental transmittance spectra at normal incidence of plasmonic arrays (NPs size 115 nm). The lattice parameter is 500 nm, mold hole size 280 nm. NPs concentration: a, c) 30 mM Au^0 b, d) 10 mM Au^0. c,d) Grey lines experimental transmittance spectra before index match. Green and Red lines experimental transmittance spectra after index match, arrays corresponding to panel a and b respectively, e) calculated transmittance spectra of dimer (black line) and trimer (red line) arrays of 115 nm particles.*

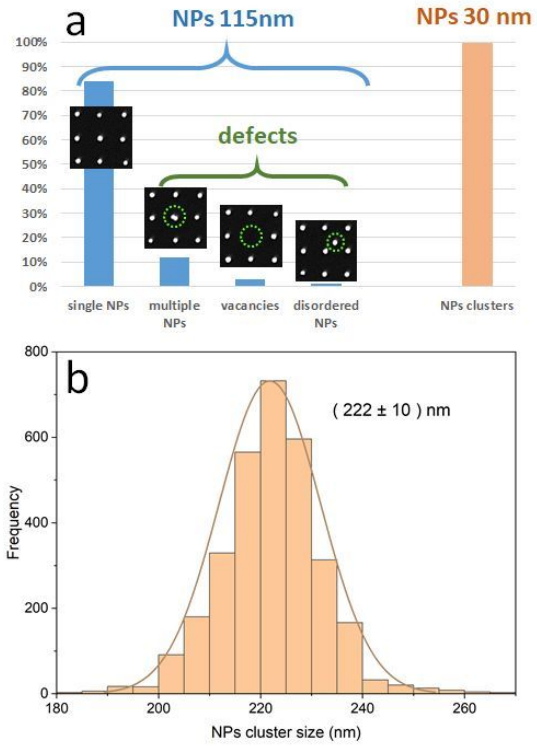

Figure S6 *Statistical analysis of Figure 3 (SEM images). a) Cells morphology quantitative distribution of 115 nm NPs array (blue bars), and 30nm NPs array (orange bar). b) NPs clusters size distribution of 30 nm NPs array.*

The statistical analysis of the SEM images (**Figure S6**) from single 115 nm single particle versus 30 nm Au clusters shows the abundance of defects present in the large colloid assembly respect to the rather homogeneous assembly that can be achieved in the case of the small particles which translates in the better optical response of the latter system.

13. Low magnification SEM images

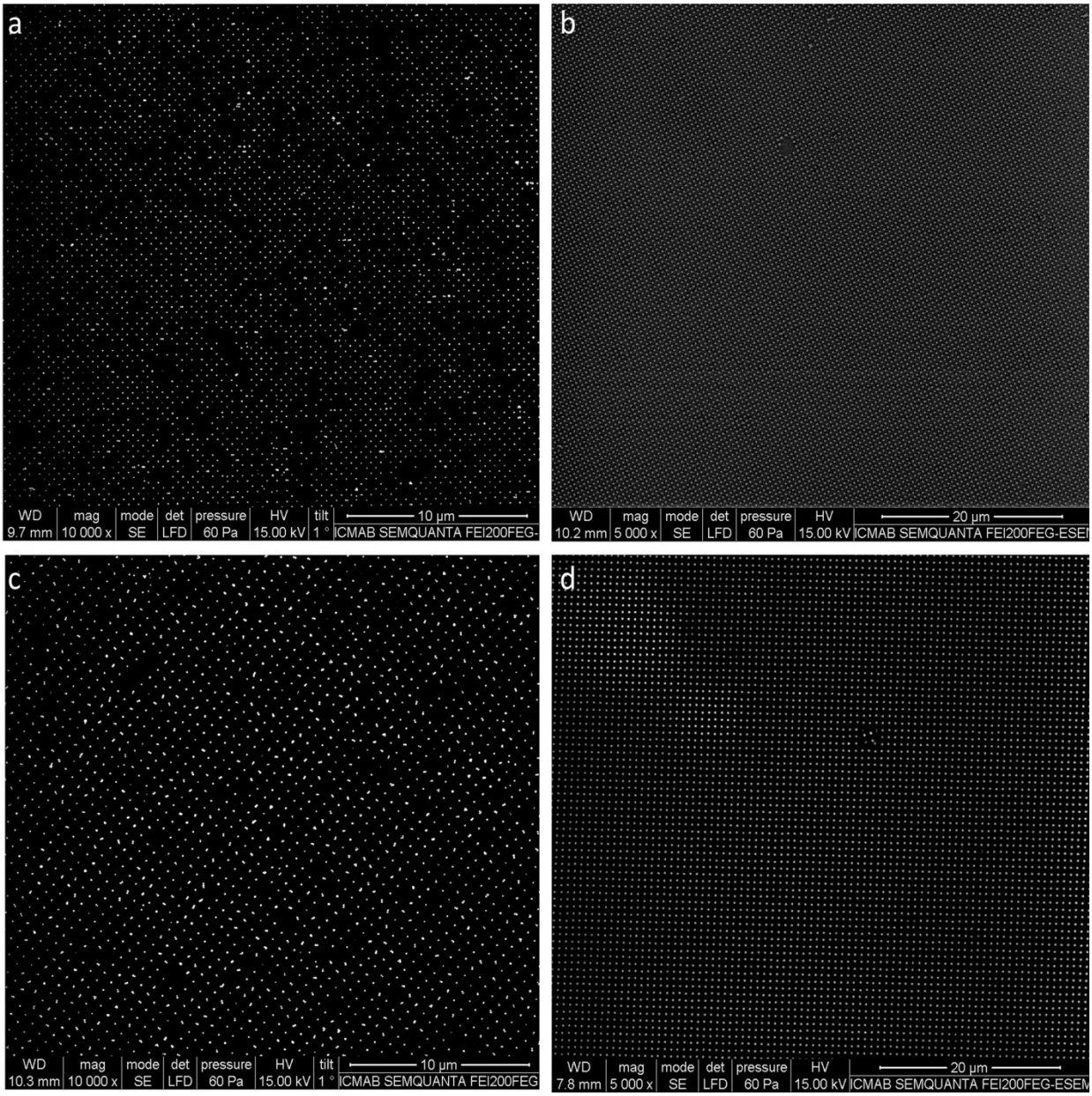

Figure S7 *Low magnification SEM image of Au NPs array. The lattice parameters (a) 400 nm, (b) 500 nm (c) 600 nm (d) 760 nm. NPs size are 115 nm (a, c) and 30 nm (b, d).*

14. Nanoparticle cluster size effects on the optical properties of the arrays.

In this section, a combined theoretical and experimental study is undertaken to elucidate the interplay of nanoparticle cluster size on the optical response of the arrays. Initially, a series of calculations are presented for lattices of 28 nm Au NPs clusters supported on a substrate with a refractive index of $n_1 = 1.43$ and LP fixed at 500 nm. We have varied the number of NPs composing each cluster, which affects the scatterer's size for a fixed LP. The inset of Figure S8a provides a scheme of the modeled clusters for each curve: 7 NPs (diameter: 90 nm) correspond to the black frame, while 19, 37, and 50 NPs (150 nm, 210 nm, and 250 nm in diameter) represent the red, green, and magenta frames, respectively. Notably, for the cluster comprised of 50 NPs, a second layer is considered.

Transmittance spectra before index match are illustrated in Figure S8a (with the superstrate having a refractive index of $n_2 = 1$). Across all curves, the presence of the LSPR of the cluster is observed, localized at 570 nm for the smallest cluster. As the cluster size increases, the mode shifts towards longer wavelengths, accompanied by higher extinction (lower transmittance). Notably, a shoulder at 662 nm emerges for the 210 nm cluster (green line), which, for the larger cluster, is resolved into a distinct second band. This mode can be attributed to far-field coupling between the clusters, constituting a collective mode of the array. The prominence of this behavior for larger clusters is conjectured to stem from their heightened scattering ability, enabling the sustenance of modes of this nature.

Figure S8b shows the transmittance spectra corresponding to the previously examined structures after index matching ($n_2 = 1.43$). Distinct spectral features are discernible; first and second-order RAs are observed at 715 nm and 505 nm, respectively. The LSPR of the cluster redshift from 605 nm (black curve) to 644 nm (magenta curve) as the cluster size increases, concomitant with an increase in the bandwidth. Remarkably the SLR appears at wavelengths slightly beyond λ_{RA}. The spectral characteristics (Q-Factor) of the SLR strongly depend on the NP cluster size (as detailed in the inset table of Figure S8b). A discernible bathochromic shift in λ_{SLR}, concomitant with a substantial broadening of the resonance, is evident as the cluster size increases. The Q-factor of the SLR undergoes a pronounced growth for smaller clusters. In stark contrast, the resonance amplitude diminishes notably, registering more than a fourfold decrease for the smallest cluster relative to the largest.

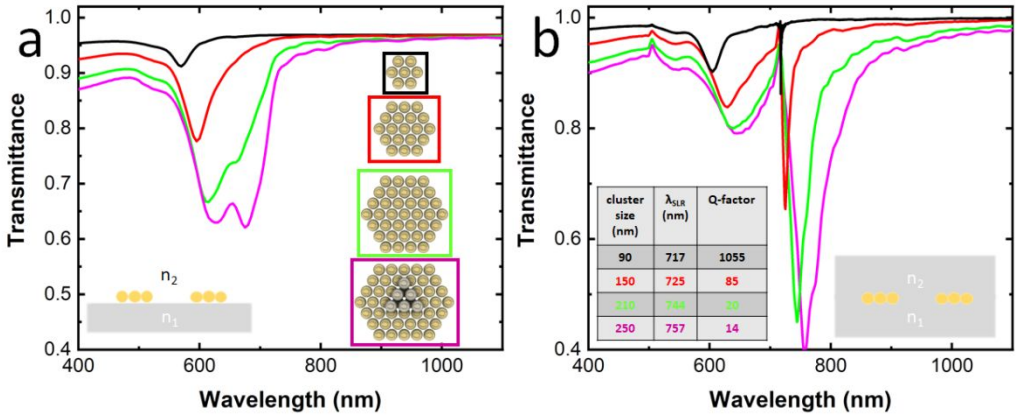

Figure S8 *FDTD calculated transmittance spectra a) before and b) after index match at normal incidence of plasmonic arrays (NPs size 28 nm) with increasing NPs cluster size. The lattice parameter is 500 nm in all cases. Panel a inset: schemes of the modeled clusters for each transmittance curve: 7 NPs (diameter: 90 nm) black, while 19, 37, and 50 NPs (150 nm, 210 nm, and 250 nm) represent the red, green, and magenta lines, respectively. Panel b inset: summary of SLR spectral properties.*

Figure S9 presents the experimental illustration of the previous theoretical study, the evolution of the transmittance spectra (with SEM images) for NP arrays with an identical LP and increasing cluster sizes. The evolution of optical properties with cluster size for the nanostructures before index match (Figure S9a, d, g) mirrors the computational trend. Larger cluster sizes correspond to the emergence of a secondary spectral band in the transmittance spectrum at longer wavelengths relative to the cluster LSPR. Post-index matching, the RAs become evident, and the SLR emerges, with the broadening and amplitude of the resonances exhibiting similarities to the trends predicted by computational results.

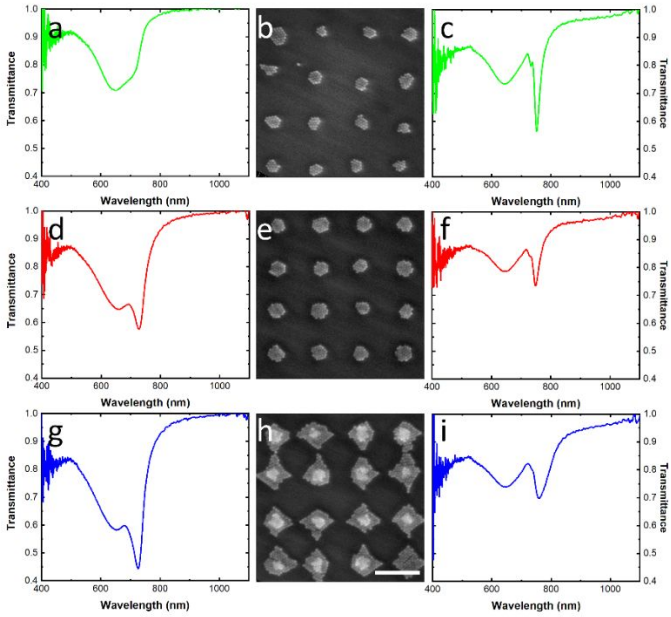

Figure S9 *Experimental transmittance spectra at normal incidence of plasmonic arrays (NPs size 30 nm) with increasing NPs cluster size. The lattice parameter is 500 nm. Objective NA = 0.1. Transmittance is shown both before index matching (a, d, g) and after index matching (c, f, i). Representative SEM images are provided in (b, e, h) with a scale bar of 500 nm.*

15. Angular characterization of meta-molecule arrays

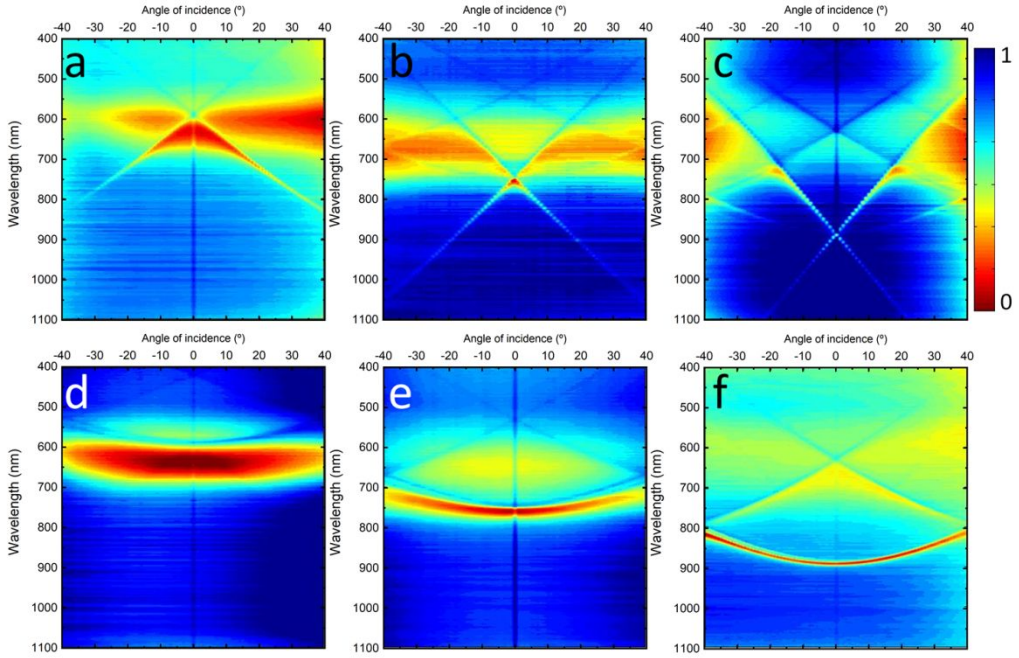

Figure S10 *Normalized angle-resolved transmittance map measured with s-polarized (a - c) and p-polarized (d - f) incident light. Sample lattice parameter 400 nm (a, d), 500 nm (b, e), 600 nm (c, f).*

16. Transmittance spectra under coherent light source illumination

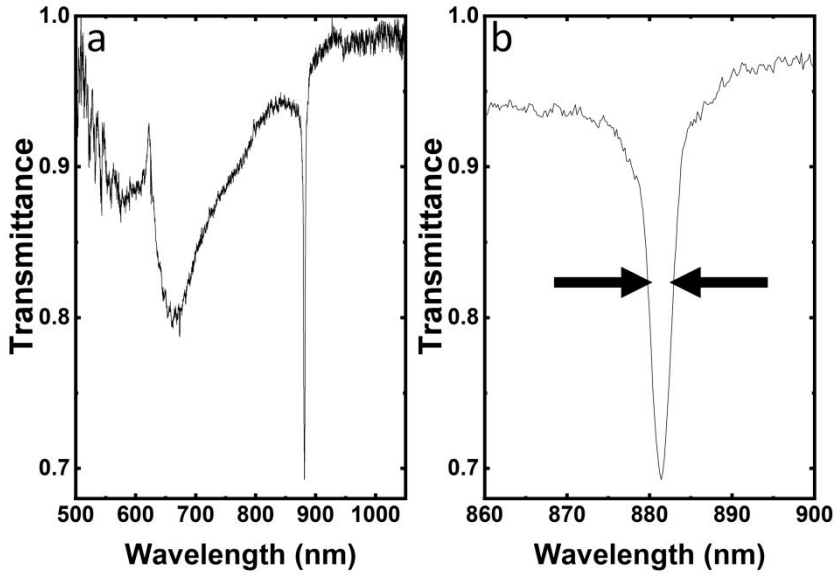

Figure S11 *a, b) Experimental transmittance spectra at normal incidence of plasmonic meta-molecule arrays (NPs size 30 nm). Lattice parameter: 600 nm. Q-factor = 291, $\Delta\lambda$ = 3.02 nm. Light source: Supercontinuum Laser.*

17. Transmittance spectra in the NIR/IR spectral region

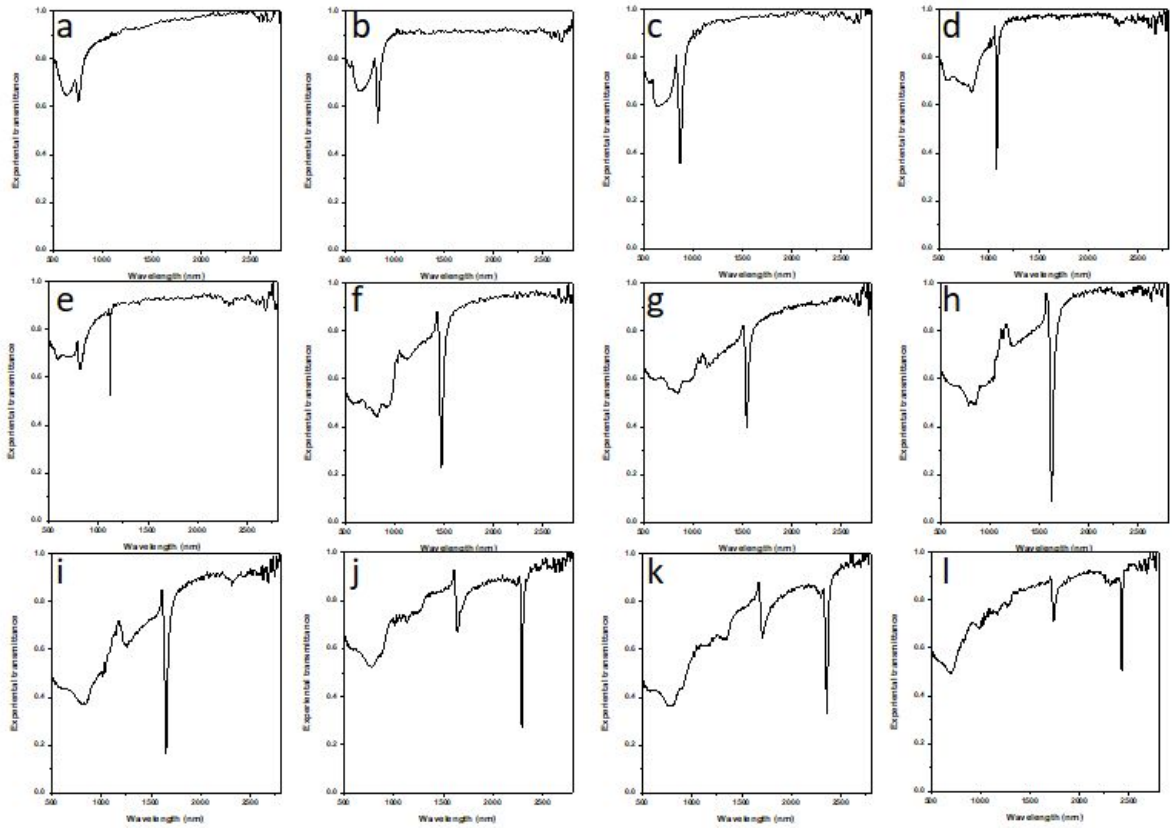

Figure S12 *a-l) Experimental transmittance spectra at normal incidence of plasmonic meta-molecule arrays (NPs size 30 nm). Lattice parameters: a) 520 nm, b) 560 nm, c) 580 nm, d) 740 nm, e) 780 nm, f) 1000 nm, g) 1060 nm, h) 1100 nm, i) 1140 nm, j) 1600 nm, k) 1660 nm, l) 1700 nm.*

18. SEM images at different magnification

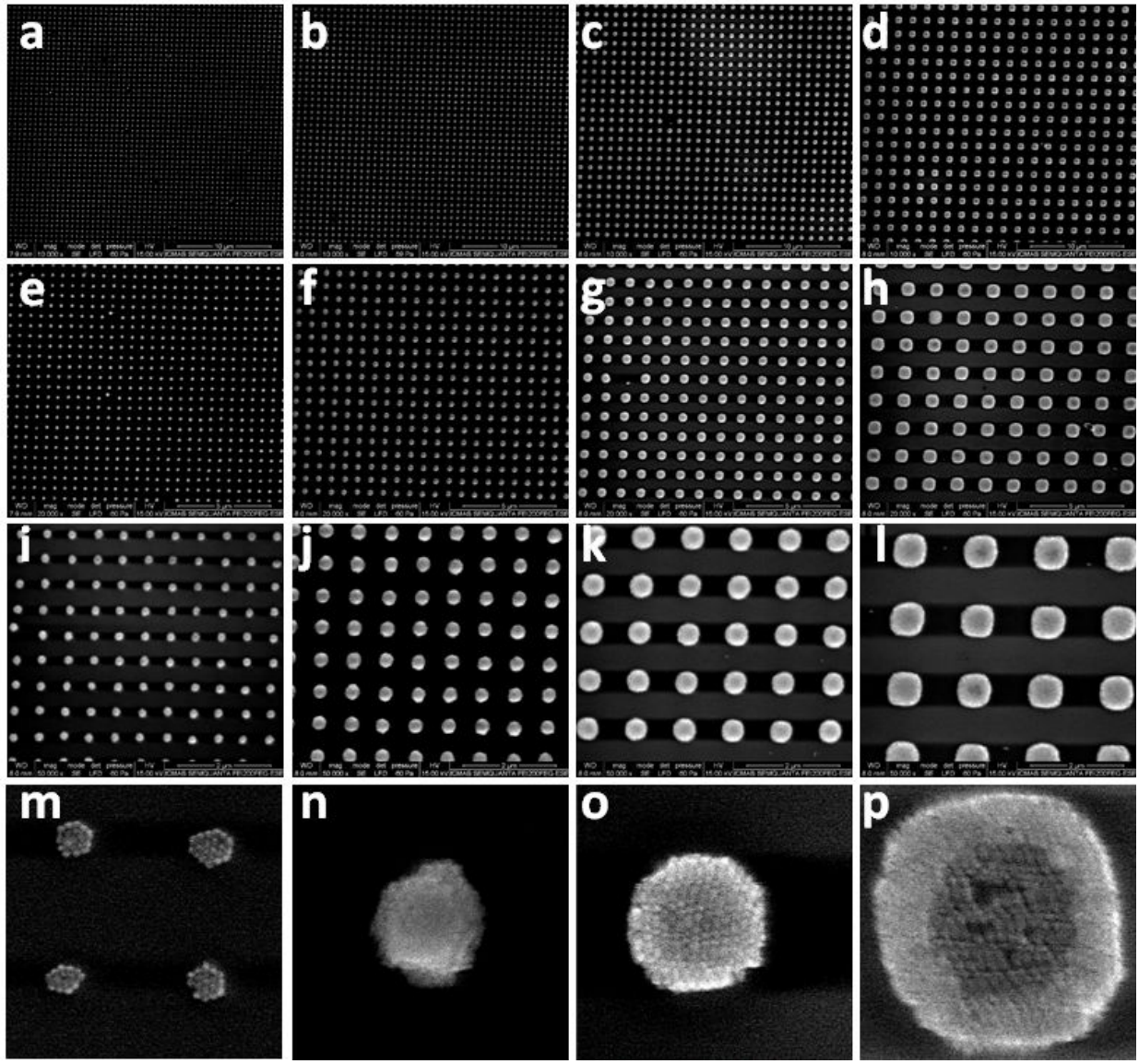

Figure S13 *a-p) SEM images of the samples corresponding to Figure 6 at different magnifications. a, e, j, m) LP = 560 nm, b, f, j, n) LP = 740 nm, c, g, k, o) LP = 1140 nm, d, h, l, p) LP = 1600 nm.*

19. Surface lattice resonances in hexagonal lattices

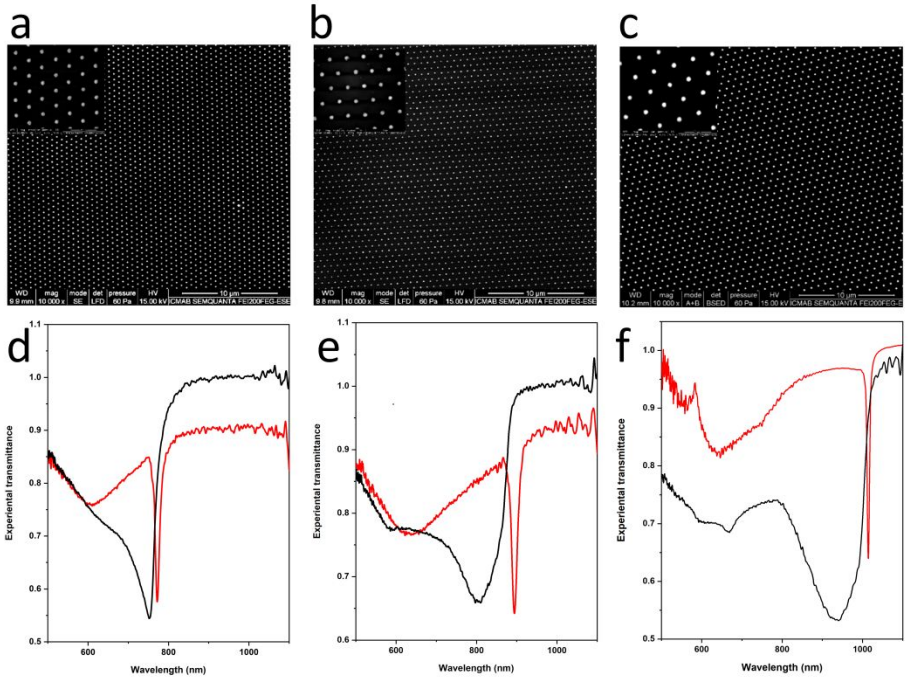

Figure S14 *a-c) SEM images and d-f) transmittance spectra at normal incidence of hexagonal lattice 30 nm NPs clusters on glass. Lattice Parameters: a, d) 600 nm, b, e) 700 nm, c, f) 800 nm. Inset: high magnification SEM images. d-f) Black lines represent the optical response before index match. Red lines represent the optical response after oil index match. Q-factors after index match: 60 (λ = 771 nm), 56 (λ = 894 nm) and 170 (λ = 1015 nm).*

20. Transmittance spectra of different samples with 600 nm lattice parameter

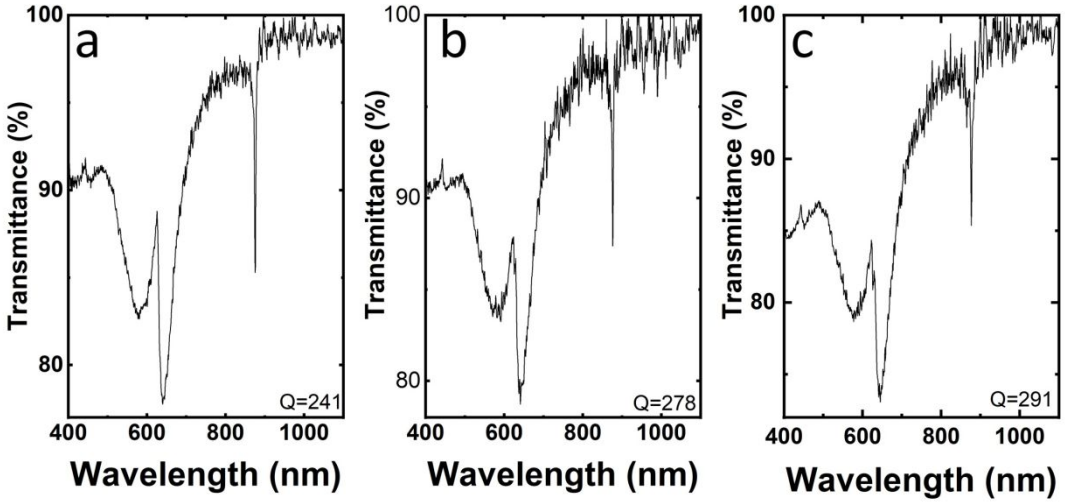

Figure S15 *a-c) Experimental transmittance spectra at normal incidence for plasmonic metamolecule arrays samples (NPs size 30 nm) equivalent to that presented in Figure 7a. Lattice parameter: 600 nm.*

21. Q-factor dependence on the angle of incidence and SLR wavelength.

In Figure S16, we present the intricate interplay between the quality factor, the angle of light incidence, and the Surface Longitudinal Resonance wavelength for diffractive modes (-1,0) and (+1,0) under s-polarized light incidence. The upper axes of the figure correspond to the λ_{SLR} values characterizing each mode.

The dispersion relation of these modes is a near-linear behavior. At normal incidence, both modes resonate at the same frequency. Subsequently, the λ_{SLR} (-1,0) shifts towards longer wavelengths, while λ_{SLR} (+1,0) shifts towards shorter wavelengths for positive angles, and the opposite trend for negative angles, as depicted in Figure 7c.

Furthermore, an evident dependence of the Q-factor on the angle of incidence/λ_{SLR} is observed, as illustrated in Figure S16. Both modes depict a non-symmetric Q-factor dependence with respect to positive and negative angles. In general terms, the Q-factor decreases faster as we deviate from the normal, resulting in smaller λ_{SLR} values when compared with the alternate branch (longer λ_{SLR}). The differences in the behavior can be understood in terms of the coupling strength between the LSPR and the RA, and the losses of the modes.[11]

At shorter wavelengths, in proximity to the LSPR, greater losses lead to a pronounced reduction in Q-factor values. For instance, at an incidence angle of 10 degrees, the Q-factor associated with the diffraction mode (+1,0) (or -10 degrees for (-1,0)) decreased to approximately 70. In contrast, at longer wavelengths, the Q-factor decay rate is more gradual, decreasing by less than a factor of 2 for a λ_{SLR} = 975 nm (at an inclination of ±10 degrees). This trend in the Q-factor can be attributed to different dispersion coupling strength between the LSPR and the RA, modulating the Q-factor values but fundamentally, it emerges as a diminishment of the resonance amplitude (see Figure 7c).

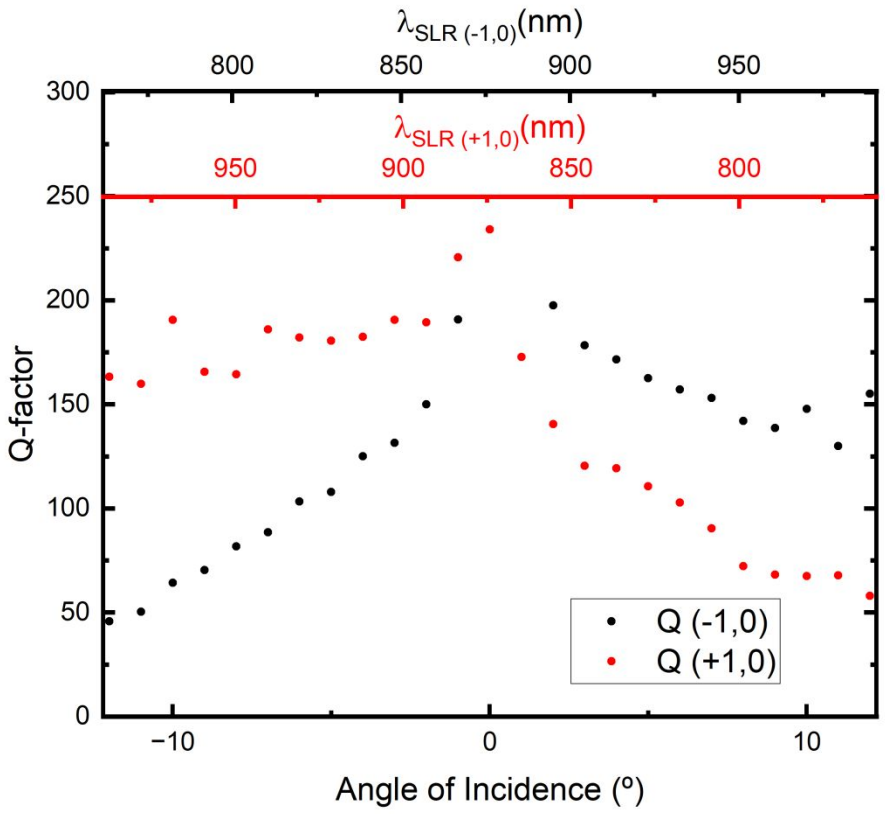

Figure S16 *Experimental Q-factor dependence on the angle of incidence and the SLR wavelength (λ_{SLR}), for the (-1,0) and (+1,0) diffraction modes, in plasmonic meta-molecule arrays made with 30 nm Au nanoparticles, with lattice parameters of 600 nm. The measurements were conducted under s-polarized incident light, as illustrated in Figure 7c.*

References

1. Hanske, C.; González-Rubio, G.; Hamon, C.; Formentín, P.; Modin, E.; Chuvilin, A.; Guerrero-Martínez, A.; Marsal, L. F.; Liz-Marzán, L. M., Large-scale Plasmonic Pyramidal Supercrystals via Templated Self-Assembly of Monodisperse Gold Nanospheres. *J. Phys. Chem. C* **2017,** *121* (20), 10899-10906.
2. Scarabelli, L.; Sanchez-Iglesias, A.; Perez-Juste, J.; Liz-Marzan, L. M., A "Tips and Tricks" Practical Guide to the Synthesis of Gold Nanorods. *J. Phys. Chem. Lett.* **2015,** *6* (21), 4270-4279.
3. Colomer-Ferrer, O.; Toda Cosi, S.; Conti, Y.; Medina-Quiroz, D. E.; Scarabelli, L.; Mihi, A., Pre- and Post-assembly Modifications of Colloidal Plasmonic Arrays: the Effect of Size Distribution, Composition and Annealing. *J. Mater. Chem. C* **2022,** *10* (37), 13913-13921.
4. Rodriguez, S. R. K.; Schaafsma, M. C.; Berrier, A.; Gómez Rivas, J., Collective Resonances in Plasmonic Crystals: Size Matters. *Physica B: Condensed Matter* **2012,** *407* (20), 4081-4085.
5. Zundel, L.; Deop-Ruano, J. R.; Martinez-Herrero, R.; Manjavacas, A., Lattice Resonances Excited by Finite-Width Light Beams. *ACS Omega* **2022,** *7* (35), 31431-31441.
6. Bin-Alam, M. S.; Reshef, O.; Mamchur, Y.; Alam, M. Z.; Carlow, G.; Upham, J.; Sullivan, B. T.; Menard, J. M.; Huttunen, M. J.; Boyd, R. W.; Dolgaleva, K., Ultra-high-Q Resonances in Plasmonic Metasurfaces. *Nat. Commun.* **2021,** *12* (1), 974.

7. Cherqui, C.; Bourgeois, M. R.; Wang, D.; Schatz, G. C., Plasmonic Surface Lattice Resonances: Theory and Computation. *Acc. Chem. Res.* **2019,** *52* (9), 2548-2558.
8. Auguié, B.; Bendaña, X. M.; Barnes, W. L.; García de Abajo, F. J., Diffractive Arrays of Gold Nanoparticles Near an Interface: Critical Role of the Substrate. *Phys. Rev. B* **2010,** *82* (15), 155447.
9. Auguié, B.; Barnes, W. L., Diffractive Coupling in Gold Nanoparticle Arrays and the Effect of Disorder. *Opt. Lett.* **2009,** *34* (4), 401-403.
10. Molet, P.; Passarelli, N.; Pérez, L. A.; Scarabelli, L.; Mihi, A., Engineering Plasmonic Colloidal Meta-molecules for Tunable Photonic Supercrystals. *Adv. Opt. Mater.* **2021,** 9 (20), 2100761.
11. Le-Van, Q.; Zoethout, E.; Geluk, E. J.; Ramezani, M.; Berghuis, M.; Gómez Rivas, J., Enhanced Quality Factors of Surface Lattice Resonances in Plasmonic Arrays of Nanoparticles. *Adv. Opt. Mater.* **2019,** *7* (6), 1801451.